# 3D imaging of biofilms on implants by detection of scattered light with a scanning laser optical tomograph

**Marko Heidrich,[1,3,*] Mark P. Kühnel,[2] Manuela Kellner,[2] Raoul-Amadeus Lorbeer,[1] Tineke Lange,[2] Andreas Winkel,[2,5] Meike Stiesch,[2] Heiko Meyer,[1,4] and Alexander Heisterkamp[1,3]**

[1] *Biomedical Optics Department, Laser Zentrum Hannover e.V., Hollerithallee 8, D-30419 Hannover, Germany;*

[2] *Department of Prosthetic Dentistry and Biomedical Materials Science, Hannover Medical School, Carl-Neubergstr.1, D-30625 Hannover, Germany;*

[3] *Institute of Quantum Optics, Gottfried Wilhelm Leibniz Universität Hannover, Welfengarten1, D-30167 Hannover, Germany;*

[4] *Department of Cardiothoracic, Transplantation and Vascular Surgery, Hannover Medical School, Carl-Neubergstr.1, D-30625 Hannover, Germany;*

[5] *CrossBIT Verbundzentrum für Biokompatibilität und Implantatimmunologie in der Medizintechnik, Feodor-Lynen-Straße 31, D-30625 Hannover, Germany;*

**M.Heidrich@lzh.de*

**Abstract:** Biofilms – communities of microorganisms attached to surfaces – are a constant threat for long-term success in modern implantology. The application of laser scanning microscopy (LSM) has increased the knowledge about microscopic properties of biofilms, whereas a 3D imaging technique for the large scale visualization of bacterial growth and migration on curved and non-transparent surfaces is not realized so far.

Towards this goal, we built a scanning laser optical tomography (SLOT) setup detecting scattered laser light to image biofilm on dental implant surfaces. SLOT enables the visualization of living biofilms in 3D by detecting the wavelength-dependent absorption of non-fluorescent stains like e.g. reduced triphenyltetrazolium chloride (TTC) accumulated within metabolically active bacterial cells. Thus, the presented system allows the large scale investigation of vital biofilm structure and *in vitro* development on cylindrical and non-transparent objects without the need for fluorescent vital staining. We suggest SLOT to be a valuable tool for the structural and volumetric investigation of biofilm formation on implants with sizes up to several millimeters.



**OCIS codes:** (110.0110) Imaging systems; (180.0180) Microscopy; (290.0290) Scattering; (180.5810) Scanning microscopy; (180.6900) Three-dimensional microscopy; (110.6955) Tomographic imaging;

## References

1. G. G. Anderson and G. A. O'Toole, "Innate and induced resistance mechanisms of bacterial biofilms," Curr. Top. Microbiol. Immunol. **322**, 85–105 (2008).
2. W. Heuer, A. Kettenring, S. N. Stumpp, J. Eberhard, E. Gellermann, A. Winkel, and M. Stiesch, "Metagenomic analysis of the peri-implant and periodontal microflora in patients with clinical signs of gingivitis or mucositis," Clin. Oral Invest. (to be published), http://www.springerlink.com/content/g1r731m87777jt43/.

#152496 - $15.00 USD Received 8 Aug 2011; revised 2 Sep 2011; accepted 2 Sep 2011; published 3 Oct 2011

3. T. Beikler and T. F. Flemmig, "Oral biofilm-associated diseases: trends and implications for quality of life, systemic health and expenditures," Periodontology 2000 **55**, 87–103 (2011).
4. N. U. Zitzmann and T. Berglundh, "Definition and prevalence of peri-implant diseases," J. Clin. Periodontol. **35**, 286–291 (2008).
5. J. R. Lawrence, D. R. Korber, B. D. Hoyle, J. W. Costerton, and D. E. Caldwell, "Optical sectioning of microbial biofilms." J. Bacteriol. **173**, 6558–6567 (1991).
6. T. R. Neu, B. Manz, F. Volke, J. J. Dynes, A. P. Hitchcock, and J. R. Lawrence, "Advanced imaging techniques for assessment of structure, composition and function in biofilm systems," FEMS Microbiol. Ecol. **72**, 1–21 (2010).
7. E. Morgenroth and K. Milferstedt, "Biofilm engineering: linking biofilm development at different length and time scales," Rev. Environ. Sci. Bio/Technology **8**, 203–208 (2009).
8. T. J. Battin, W. T. Sloan, S. Kjelleberg, H. Daims, I. M. Head, T. P. Curtis, and L. Eberl, "Microbial landscapes: new paths to biofilm research," Nat. Rev. Microbiol. **5**, 76–81 (2007).
9. J. M. Tyszka, S. E. Fraser, and R. E. Jacobs, "Magnetic resonance microscopy: recent advances and applications," Curr. Opinion Biotechnol. **16**, 93–99 (2005).
10. B. Manz, F. Volke, D. Goll, and H. Horn, "Measuring local flow velocities and biofilm structure in biofilm systems with magnetic resonance imaging (MRI)," Biotechnol. Bioeng. **84**, 424–432 (2003).
11. J. D. Seymour, S. L. Codd, E. L. Gjersing, and P. S. Stewart, "Magnetic resonance microscopy of biofilm structure and impact on transport in a capillary bioreactor," J. Magn. Reson. **167**, 322–327 (2004).
12. J. S. McLean, O. N. Ona, and P. D. Majors, "Correlated biofilm imaging, transport and metabolism measurements via combined nuclear magnetic resonance and confocal microscopy," ISME J **2**, 121–131 (2007).
13. Z. Lewandowski, S. A. Altobelli, and E. Fukushima, "NMR and microelectrode studies of hydrodynamics and kinetics in biofilms," Biotechnol. Prog. **9**, 40–45 (1993).
14. D. Huang, E. A. Swanson, C. P. Lin, J. S. Schuman, W. G. Stinson, W. Chang, M. R. Hee, T. Flotte, K. Gregory, C. A. Puliafito, and J. G. Fujimoto, "Optical coherence tomography," Science **254**, 1178 –1181 (1991).
15. C. Xi, D. Marks, S. Schlachter, W. Luo, and S. A. Boppart, "High-resolution three-dimensional imaging of biofilm development using optical coherence tomography," J. Biomed. Opt. **11**, 034001 (2006).
16. C. Haisch and R. Niessner, "Visualisation of transient processes in biofilms by optical coherence tomography," Water Res. **41**, 2467–2472 (2007).
17. M. Wagner, D. Taherzadeh, C. Haisch, and H. Horn, "Investigation of the mesoscale structure and volumetric features of biofilms using optical coherence tomography," Biotechnol. Bioeng. **107**, 844–853 (2010).
18. C. T. Nguyen, H. Tu, E. J. Chaney, C. N. Stewart, and S. A. Boppart, "Non-invasive optical interferometry for the assessment of biofilm growth in the middle ear," Biomed. Opt. Express **1**, 1104–1116 (2010).
19. R. Lorbeer, M. Heidrich, C. Lorbeer, D. F. Ramírez Ojeda, G. Bicker, H. Meyer, and A. Heisterkamp, "Highly efficient 3D fluorescence microscopy with a scanning laser optical tomograph," Opt. Express **19**, 5419–5430 (2011).
20. J. Sharpe, U. Ahlgren, P. Perry, B. Hill, A. Ross, J. Hecksher-Sørensen, R. Baldock, and D. Davidson, "Optical projection tomography as a tool for 3D microscopy and gene expression studies," Science **296**, 541 –545 (2002).
21. J. Gabrielson, M. Hart, A. Jarelöv, I. Kühn, D. McKenzie, and R. Möllby, "Evaluation of redox indicators and the use of digital scanners and spectrophotometer for quantification of microbial growth in microplates," J. Microbiol. Methods **50**, 63–73 (2002).
22. E. Kun and L. G. Abood, "Colorimetric estimation of succinic dehydrogenase by triphenyltetrazolium chloride," Science **109**, 144 –146 (1949).
23. R. Kuhn and D. Jerchel, "Über Invertseifen, VIII. mitteil.: Reduktion von Tetrazoliumsalzen durch Bakterien, gärende Hefe und keimende Samen," Ber. Dtsch. Chem. Ges. A B **74**, 949–952 (1941).
24. P. L. Steponkus and F. O. Lanphear, "Refinement of the triphenyl tetrazolium chloride method of determining cold injury," Plant Physiol. **42**, 1423 –1426 (1967).
25. S. Bolte and F. P. Cordelières, "A guided tour into subcellular colocalization analysis in light microscopy," J. Microsc. **224**, 213–232 (2006).
26. H. Meyer, A. Garofalakis, G. Zacharakis, S. Psycharakis, C. Mamalaki, D. Kioussis, E. N. Economou, V. Ntziachristos, and J. Ripoll, "Noncontact optical imaging in mice with full angular coverage and automatic surface extraction," Appl. Opt. **46**, 3617–3627 (2007).
27. J. R. Walls, J. G. Sled, J. Sharpe, and R. M. Henkelman, "Correction of artefacts in optical projection tomography," Phys. Med. Biol. **50**, 4645–4665 (2005).
28. J. W. Goodman, "Some fundamental properties of speckle," J. Opt. Soc. Am. **66**, 1145–1150 (1976).
29. R. Lorbeer, H. Meyer, M. Heidrich, H. Lubatschowski, and A. Heisterkamp, "Applying optical Fourier filtering to standard optical projection tomography," Proc. SPIE **7570**, 75700 (2010).
30. J. R. Walls, J. G. Sled, J. Sharpe, and R. M. Henkelman, "Resolution improvement in emission optical projection tomography," Phys. Med. Biology **52**, 2775–2790 (2007).
31. W. Drexler and J. G. Fujimoto, *Optical Coherence Tomography: Technology and Applications* (Springer, New York, 2008).
32. H. Meyer, A. Darrell, A. Metaxakis, C. Savakis, and J. Ripoll, "Optical projection tomography for in-vivo imaging of drosophila melanogaster," Microsc. Anal. **22**, 19–22 (2008).

#152496 - $15.00 USD Received 8 Aug 2011; revised 2 Sep 2011; accepted 2 Sep 2011; published 3 Oct 2011

33. H. Meyer, "Optical projection tomography in biological model organisms," Ph.D. thesis (Erasmus Universiteit, Rotterdam, Netherlands, 2010).
34. U. J. Birk, M. Rieckher, N. Konstantinides, A. Darrell, A. Sarasa-Renedo, H. Meyer, N. Tavernarakis, and J. Ripoll, "Correction for specimen movement and rotation errors for in-vivo optical projection tomography," Biomed. Opt. Express **1**, 87–96 (2010).
35. M. Rieckher, U. J. Birk, H. Meyer, J. Ripoll, and N. Tavernarakis, "Microscopic optical projection tomography in vivo," PLoS One **6**, e18963 (2011).
36. J. McGinty, H. B. Taylor, L. Chen, L. Bugeon, J. R. Lamb, M. J. Dallman, and P. M. W. French, "In vivo fluorescence lifetime optical projection tomography," Biomed. Opt. Express **2**, 1340–1350 (2011).
37. K. Subramani, R. E. Jung, A. Molenberg, and C. H. F. Hammerle, "Biofilm on dental implants: a review of the literature," Int. J. Oral Maxillofacial Implants **24**, 616–626 (2009).
38. R. P. Tengerdy, J. G. Nagy, and B. Martin, "Quantitative measurement of bacterial growth by the reduction of tetrazolium salts," Appl. Microbiol. **15**, 954–955 (1967).
39. M. Burmølle, J. S. Webb, D. Rao, L. H. Hansen, S. J. Sørensen, and S. Kjelleberg, "Enhanced biofilm formation and increased resistance to antimicrobial agents and bacterial invasion are caused by synergistic interactions in multispecies biofilms," Appl. Environ. Microbiol. **72**, 3916–3923 (2006).
40. M. Kuehn, M. Hausner, H. Bungartz, M. Wagner, P. A. Wilderer, and S. Wuertz, "Automated confocal laser scanning microscopy and semiautomated image processing for analysis of biofilms," Appl. Environ. Microbiol. **64**, 4115–4127 (1998).
41. A. Heydorn, A. T. Nielsen, M. Hentzer, C. Sternberg, M. Givskov, B. K. Ersbøll, and S. Molin, "Quantification of biofilm structures by the novel computer program COMSTAT," Microbiology **146**, 2395 –2407 (2000).
42. H. Beyenal, C. Donovan, Z. Lewandowski, and G. Harkin, "Three-dimensional biofilm structure quantification," J. Microbiol. Methods **59**, 395–413 (2004).
43. H. Daims, S. Lücker, and M. Wagner, "daime, a novel image analysis program for microbial ecology and biofilm research," Environ. Microbiol. **8**, 200–213 (2006).

## 1. Introduction

Bacteria and other microorganisms like fungi, algae and protozoa are able to form interface-attached sessile communities of multispecies diversity embedded within a matrix of extracellular polymeric substances (EPS). These so-called biofilms are ubiquitous and appear frequently resistant against host immune defense or medical treatments due to the combination of different bacterial characteristics and multiple functions of protective matrices [1]. Subsequent biofilm-associated inflammation (e.g. peri-implantitis in prosthetic dentistry [2]) may lead to tissue degeneration, implant loss or dislocation of pathogens with severe systemic consequences for the patient and high costs for the health care system [3, 4].

Investigation of biofilm using laser scanning microscopy (LSM) has been well-established during the last decades [5, 6]. Its capability to perform three dimensional imaging with high resolution has improved the understanding of the structure and interactions within biofilms at the microscale. However, answering questions regarding biofilm formation at different scales and its overall ecosystem might not be possible based on microscale investigations [7]. Biofilm growth, mass transfer and detachment for example are system dependent: Choosing surfaces with specific morphology, roughness and biochemical properties can influence the biofilm development. Recently, biofilms were presented to be microbial landscapes [8]. Therefore current biofilm research requires imaging techniques filling the gap between micro- and macroscale. For the investigation of this range, termed mesoscale, particularly two techniques have been applied so far: Magnetic resonance microscopy (MRM), which is magnetic resonance imaging (MRI) at microscopic level, resolves biofilm structures with an isotropic resolution (< 100 µm, rarely less than 10 µm, [9]) and allows sample sizes of several millimeters in diameter [10, 11, 12, 13]. Optical coherence tomography (OCT) [14], on the other hand, has the ability to image biofilm within glass tubes at the mesoscale with spatial resolutions in the lower µm-range (< 20 µm) which was shown several times [15, 16, 17]. Detection and quantification of biofilm in the middle ear was demonstrated by the application of low coherence interferometry (LCI) *in vivo* [18].

Recently, we introduced scanning laser optical tomography (SLOT) [19] which can be seen

#152496 - $15.00 USD Received 8 Aug 2011; revised 2 Sep 2011; accepted 2 Sep 2011; published 3 Oct 2011

as an improvement of optical projection tomography (OPT) [20] in terms of homogeneous illumination, prevention of ring artifacts and increase of photon collection efficiency. Due to its characterizing integration with a high numerical aperture (NA) in the detection path, the generation of laser speckles is suppressed. Thus, in contrast to OPT, scattered laser light can be used as contrast mechanism in SLOT.

Here we demonstrate the utility of SLOT to image biofilms *in vitro* in the special case of biofilm-covered non-transparent surfaces with cylindrical shape. SLOT detects scattered laser light from the sample at two different wavelengths to generate a pair of projection image data sets. This is used to calculate a difference signal data set which is reconstructed subsequently to achieve a volumetric stack of the biofilm.

Moreover a new sample preparation is introduced that matches the requirements of the SLOT setup and is suitable for the *in vitro* investigation of biofilm formation on metal surfaces: Bacteria are initially applied at one end of an implant that is mounted within agarose gel containing nutrients and a redox indicator as non-fluorescent viability staining e.g. triphenyltetrazolium chloride (TTC) [21, 22, 23]. Our results suggest the combination of this *in vitro* test model with SLOT to be a valuable tool in biofilm research and dental implant material science.

## 2. Materials and Methods

### *2.1. SLOT Setup*

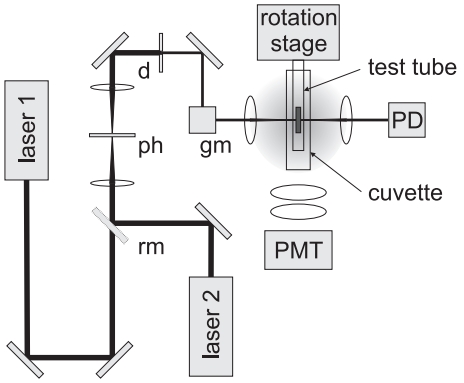


Figure 1. SLOT setup. A removable mirror (rm) allows one to choose between two laser sources, a helium-neon laser and a green laser module, respectively. The spatially cleaned and aperture-adjusted laser beam is scanned through the sample which is mounted rotatably in a glass test tube positioned in a cuvette filled with water. Scattered laser light that is emitted to the bottom of the cuvette and reflected from its walls is focused onto a photomultiplier tube (PMT). Transmitted light is captured by a photodiode (PD). ph: pinhole; d: diaphragm; gm: x-y galvo mirror.

The SLOT setup (Fig. 1) allows to switch between two laser sources, a helium-neon (HeNe) laser (633 nm, 2 mW) and a green laser module (532 nm, 10 mW), respectively. The laser is spatially cleaned by a pinhole in a telescope and directed onto a x-y-scanning mirror system which is positioned in the back focal plane of an aspheric imaging lens with a focal length of 30 mm. A diaphragm before the scanner is used to adjust the aperture of the beam which is then focused into the sample chamber. In all experiments the chamber is a glass cuvette filled with water. The sample is mounted in a glass test tube rotatably positioned in the cuvette by a mechanical rotation stage. This setup allows acquisition of projection images from multiple viewing angles. Scattered light from the sample is detected by a photomultiplier tube (PMT) (R6357, HAMAMATSU Photonics K. K., Japan) located below the cuvette. For this purpose a

#152496 - $15.00 USD Received 8 Aug 2011; revised 2 Sep 2011; accepted 2 Sep 2011; published 3 Oct 2011

lens system consisting of two lenses with an aperture and focal length of 25 mm collects and directs scattered light onto the PMT's sensitive area. Transmitted light is collected by another imaging lens behind the chamber and detected with a photodiode (PD) to gather transmission data.

By scanning 700x700 points through the sample SLOT simultaneously acquires one transmission image from the PD signals and one scattered light image from the PMT signals within 2.7 s. Thereby, each scanned point corresponds to a projection along the optical axis. In every point, the PMT detects a fraction of the scattered light that is integrated by this projection and the PD detects transmitted light that is extenuated by the integration of absorption and scattering within the sample. All acquisitions are taken with a laser beam NA of 0.027 at 500 viewing angles.

Using scattered light detection with SLOT offers the same isotropic optical resolution of equivalent OPT setups [19]. The resolution $\Delta x = \lambda / 2\mathrm{NA}$ depends on the used laser wavelength $\lambda$ and the NA of the illumination beam that is required to cover the specimen by the depth of field (DOF). For the imaging of a non-transparent cylinder the NA is adjusted until the visible half of the implant is covered by the DOF. The required NA of 0.027 corresponds to a cylinder with a diameter of 4 mm and an illumination wavelength of 633 nm. Therefore, the isotropic optical resolution theoretically equals 12 µm.

### *2.2. Sample Preparation*

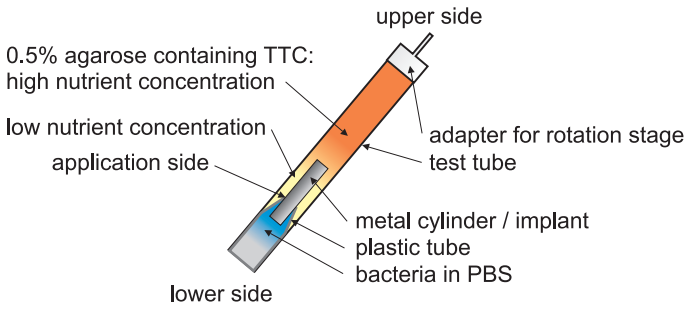


Figure 2. Prepared sample: A metal cylinder or dental implant is mounted within an agarose gel containing the redox indicator triphenyltetrazolium chloride (TTC) and a nutrient concentration gradient. A plastic tube centrically aligns the implant within the surrounding glass tube and contains the bacteria which are re-suspended in PBS. The setup allows the bacteria to migrate along the implant surface starting at the application side while having access to nutrients and TTC in the surrounding agarose gel. An adapter fixates the glass test tube with the rotation stage of the SLOT setup (Fig. 1).

The specimens are biofilms attached to cylindrical metal surfaces mounted in gel filled glass test tubes with external dimensions of 8x70 mm and a wall thickness of 0.8-1.0 mm (2613101, DURAN-Group GmbH, Germany). The used metal surfaces are either plane cylindrical titanium pins (diameter: 3 mm) or dental implants (Astra Tech AB, Sweden) made from titanium alloy (length: 18 mm, diameter: 4 mm). To sustain the metal surfaces in the test tubes the gel consists of a mixture of 0.5% agarose with added 2,3,5-triphenyltetrazolium chloride (TTC). TTC is an uncolored i.e. transparent and water soluble redox indicator that is commonly used in cell viability experiments indicating cellular respiration. In metabolically active regions in the sample where biofilm development occurs the transparent and therefore invisible TTC is reduced to red 1,3,5-triphenylformazan (TPF) which is insoluble in water. Hence, TPF accumulates within the bacterial cells and acts as a non-fluorescent stain coloring the biofilm red.

The preparation of the samples was performed as follows: All test tubes were filled with two

#152496 - $15.00 USD Received 8 Aug 2011; revised 2 Sep 2011; accepted 2 Sep 2011; published 3 Oct 2011

different agarose gels (low melting) both containing TTC. The first half of one test tube (upper part in Fig. 2) was filled with an 0.5% agarose gel containing the culture medium Tryptic Soy Broth (TSB) which provides bacterial growth. The second half was filled with an 0.5% agarose gel containing phosphate buffered saline (PBS) which has a lower nutrient concentration than the adjacent gel in the first half. As a result a nutrient concentration gradient forms. Both gels had been mixed carefully with TTC after reaching a temperature lower than 37 °C to prevent decomposition of the heat-sensitive TTC. Subsequently a metal pin or dental implant mounted in a plastic tube was immersed within the gel in order to position the sample centrically in the test tube. Biofilm-forming bacteria (*Bacillus cereus*, *Pseudomonas stutzeri* or extraction of patient's dental plaque) re-suspended in PBS were applied to one end of the mounted metal surface indicated as application side in Fig. 2. The remaining gap between metal cylinder or dental implant, respectively, and plastic tube allows the bacteria to reach the agarose and to migrate along the surface while having access to nutrients and TTC. To match the mechanical requirements of the SLOT setup an adapter fixates the glass test tube with the rotation stage.

### *2.3. Data Processing and Reconstruction*

The complete projection raw data for one point in time of a sample covers two pairs of projection data sets illuminated with 633 nm and 532 nm, respectively. Each pair consists of a set of scattered light images acquired using the PMT and a set of transmitted light images acquired using the PD. Since the imaged specimens are predominantly non-transparent, the PD signal is only an additional channel that can be used for the reconstruction of plain surfaces. Solely the scattered light signal acquired with the PMT is needed for the reconstruction of the volumetric biofilm data. The reconstruction of a projection data set containing 500 projection images was performed by using custom software which applies a filtered back projection algorithm with a ramp filter to generate a volumetric data stack.

While the normalized signal from the metal cylinder is nearly independent of the used laser wavelength, the signal from the biofilm differs due to the incorporated TPF. This is because of its high absorption in the green spectrum and the low absorption in the red spectrum [24]. Since the incident light interacting with TPF is either absorbed or scattered, the amount of scattered light at 532 nm is significantly lower than at 633 nm. Hence, the green illuminated biofilm is dark while the red illuminated biofilm is bright. Therefore the two normalized projection data sets acquired by the detection of scattered laser light were used to calculate one projection data set containing the difference signal by subtracting the green channel from the red channel. This new difference signal data set represents the biofilm without implant surface and was reconstructed as described above.

All projection data sets and volumetric data stacks were clipped and visualized with ImageJ. Rendering was performed using Voreen.

## 3. Results

We acquired multiple projection image data sets of metal cylinder and dental implant samples. Fig. 3(a,b,e,f) show selected projection images of two biofilm-covered metal cylinders each acquired by the detection of scattered light from both laser sources at the same viewing angle. The first obvious difference between a red illuminated (Fig. 3a and 3e) and a green illuminated (Fig. 3b and 3f) acquisition lies in the appearance of the biofilm: While the incorporated TPF scatters the red laser light producing a high gray value in the projection images the green laser light experiences absorption resulting in a low gray value. The agarose appears two times brighter in the green channel than in the red channel and the signal generated by scattering at the metal surface itself is nearly independent of the used illumination laser, as expected. Composite images were formed by merging red and green parts shown in Fig. 3c and 3g. As a result of the

#152496 - $15.00 USD Received 8 Aug 2011; revised 2 Sep 2011; accepted 2 Sep 2011; published 3 Oct 2011

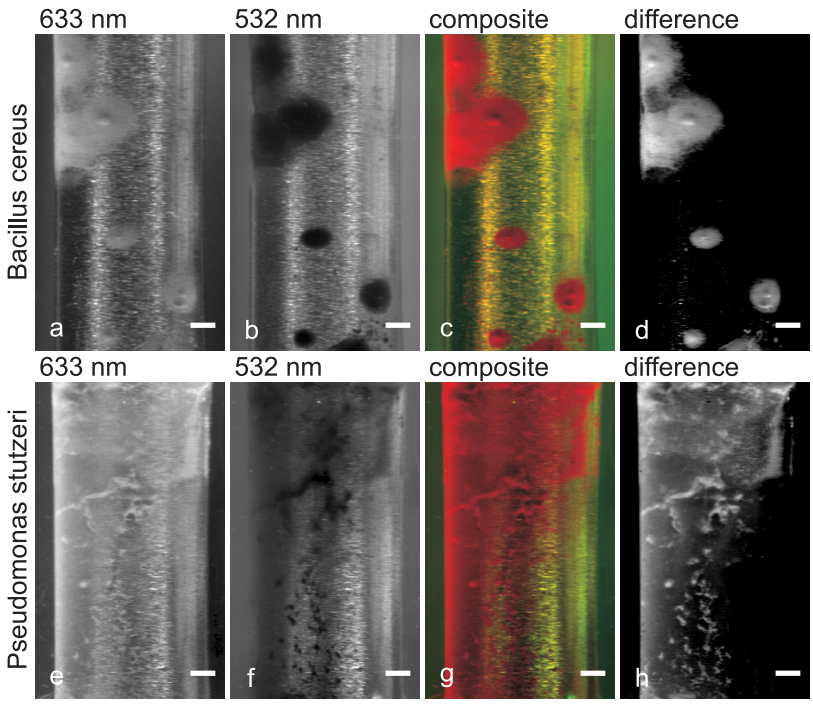


Figure 3. Projection images of two metal cylinder samples covered with biofilm consisting of *Bacillus cereus* (a-d) and *Pseudomonas stutzeri* (e-h). The samples were illuminated with both laser sources (helium-neon laser: (a,e); green laser module: (b,f)). Each image was acquired by the detection of scattered laser light at the same viewing angle. Composite images (c,g) were generated by merging red and green illuminated parts. The calculation of the difference signal provides projection images showing the biofilm only (d,h). Scale bars represent 500 µm.

missing blue channel reflective regions in the sample appear slightly yellow. Essential for subsequent reconstruction processes is the calculation of the difference signal projection images by subtracting the green channel from the red channel. These difference signal data sets solely contain signal from the biofilm covering the surface, whereas the metal surface itself is hidden. However, since the green and red channels are not exactly the same, a slight background is observed in the difference signal data sets. This is because of the wavelength-dependent scattering of the agarose gel that produces a small difference signal. Second, the green and red laser are not scattered in exactly the same way on the metal surface resulting in minor brightness differences. However, it is observed that these undesired signal differences are marginal and do not disturb the reconstruction results. In order to support the reader in comparing the projection images with the difference signal image, a threshold was set to remove the background. The result can be seen in Fig. 3d and 3h.

To investigate the ability of SLOT to image biofilm even on helical surfaces with cavity-like structures, we acquired projection image data sets of a biofilm-covered dental implant. Projection images of one viewing angle can be seen in Fig. 4a and 4b. Especially in the color merge image (Fig. 4c) (Media 1) and the difference signal image (Fig. 4d) the biofilm and its spreading along the implant surface becomes visible. The biofilm can clearly be separated from the implant independent of its position on the implant surface.

#152496 - $15.00 USD Received 8 Aug 2011; revised 2 Sep 2011; accepted 2 Sep 2011; published 3 Oct 2011

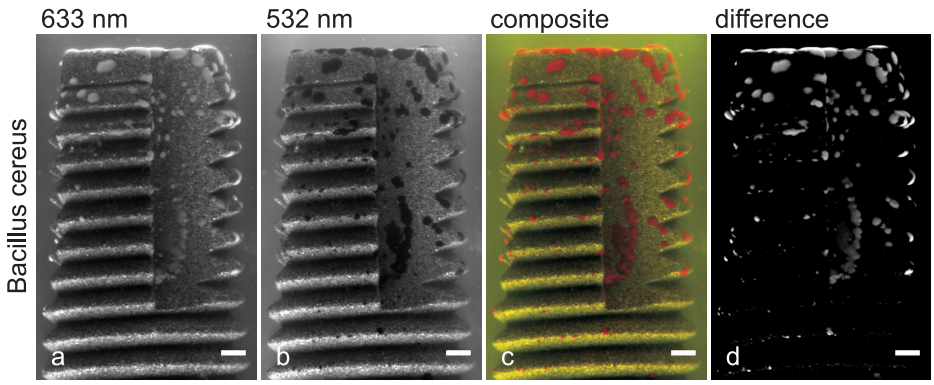


Figure 4. Projection images of a dental implant covered with biofilm consisting of *Bacillus cereus*. The samples were illuminated with both laser sources (helium-neon laser: (a); green laser module: (b)). Each image was acquired by the detection of scattered laser light at the same viewing angle. (c) is the composite image (Media 1) generated by merging (a) and (b) while the difference signal image is shown in (d). Scale bars represent 500 µm.

Directly after the initial sample preparation, the metal surfaces did not show any signs of biofilm attachment i.e. the sample was free of red stained regions. Then, depending on the used bacteria, either a thin red-stained layer appeared (*Pseudomonas stutzeri*, Fig. 3(e-h)) or clusters formed up and grew on the metal surface. In all shown projection images the nutrient concentration in the agarose gel increases from bottom to top. We observed an increase in the number of biofilm clusters and volumetric expansion in this direction, too.

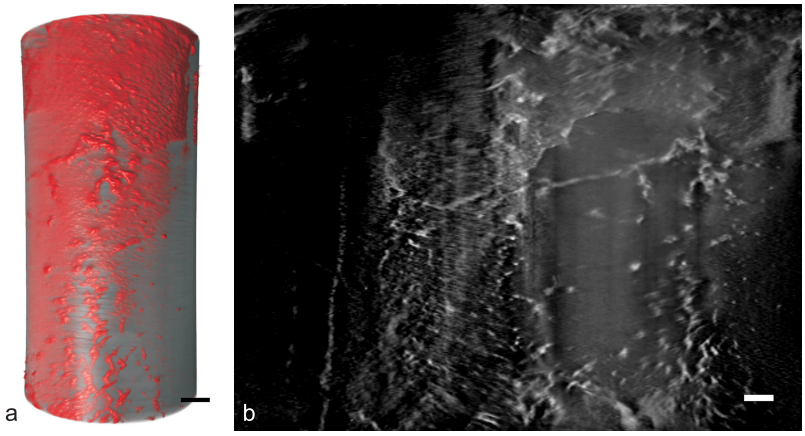


Figure 5. Reconstructed and processed volumetric stacks of the biofilm raw data shown in Fig. 3h: (a) Rendered image of the biofilm (represented in red) and the surface of the metal cylinder (gray). Difference signal data set containing the biofilm distribution and transmission data set were used for reconstruction. (b) Slice through the volumetric data stack of the biofilm along the curved cylindrical metal surface. This corresponds to a transformation of the curved cylindrical coordinates into a flat Euclidean plane. Scale bars represent 500 µm.

#152496 - $15.00 USD Received 8 Aug 2011; revised 2 Sep 2011; accepted 2 Sep 2011; published 3 Oct 2011

The difference signal data sets calculated from a pair of red and green raw data sets only contain information about the biofilm distribution. Thus, these sets can be handled like normal fluorescence data sets in emission optical projection tomography (eOPT).

We performed the reconstruction of biofilm by using the difference signal sets. For the reconstruction of the metal surface we used the transmission data sets acquired by the PD. A rendered image of the reconstructed data in Fig. 3h can be seen in Fig. 5a from a similar viewing angle. Biofilm and surface are represented in red and gray, respectively. The rendering was performed using Voreen.

Fig. 5b shows a slice through the volumetric data stack of the sample in Fig. 3h along the curved surface of the metal cylinder. This corresponds to a transformation of the curved cylindrical coordinates into a flat Euclidean plane.

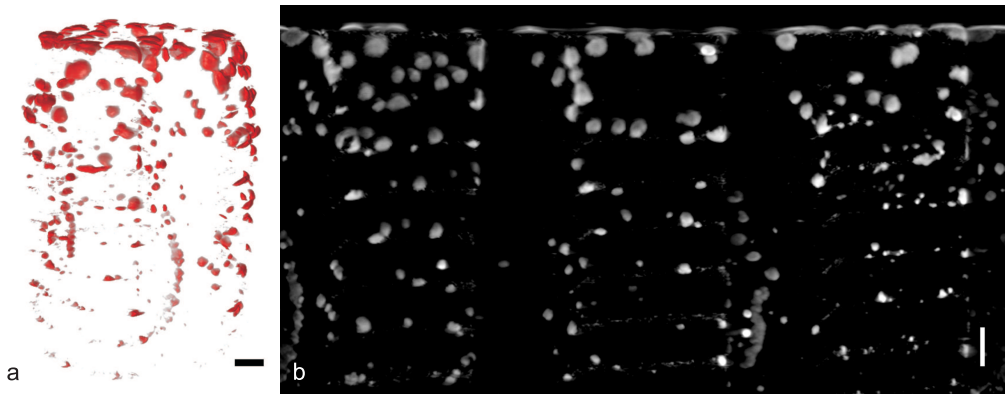


Figure 6. Reconstructed and processed volumetric stacks of the biofilm raw data shown in Fig. 4d. The difference signal data set containing the biofilm distribution was used for reconstruction. (a) Rendered image of the biofilm (represented in red) (Media 2). (b) Radial maximum intensity projection (rMIP) of the volumetric data stack of the biofilm. Scale bars represent 500 µm.

Implant surfaces with cavity-like structures cannot be reconstructed from transmission data due to shadowing effects. However, it is possible to reconstruct the biofilm covering the dental implant (Fig. 4d) by using the difference signal data set. Fig. 6 shows the reconstructed and processed volumetric data stack of this sample. A rendered image of the biofilm is displayed in Fig. 6a (Media 2) while in Fig. 6b a radial maximum intensity projection (rMIP) centered on the axis of the implant can be seen. Most of the biofilm is attached on the screw surface while only few clusters grow within the cavities.

To demonstrate that volumetric data stacks of biofilm generated with SLOT can be used for computer aided growth and development studies, we exemplarily investigated a titanium sample covered with biofilm clusters and analyzed the biofilm formation. Therefore, initially a metal cylinder was inoculated with bacteria extracted from a patient's dental plaque. Then, 48 h and 72 h after the preparation, the specimen was investigated using SLOT. The difference signal data sets of both points in time were generated and reconstructed. Maximum intensity projections (MIP) of the resulting volumetric stacks can be seen in Fig. 7a and Fig. 7c. Subsequently the stacks were analyzed using the ImageJ plugin *3D Object Counter* [25]. We achieved cluster number and cluster volume depending on the height on the implant surface. The scatter plots in Fig. 7b and Fig. 7d show the results of this investigation. First of all, the cluster number increases from 246 clusters (Fig. 7b) to 467 clusters within 24 h (Fig. 7d). Second, the volume of the clusters in the upper region is larger than in the lower region of the sample which is in

#152496 - $15.00 USD Received 8 Aug 2011; revised 2 Sep 2011; accepted 2 Sep 2011; published 3 Oct 2011

accordance with the nutrient concentration gradient in the agarose gel. Third, the number of small clusters increases within 24 h, while their distribution is independent of the height on the surface.

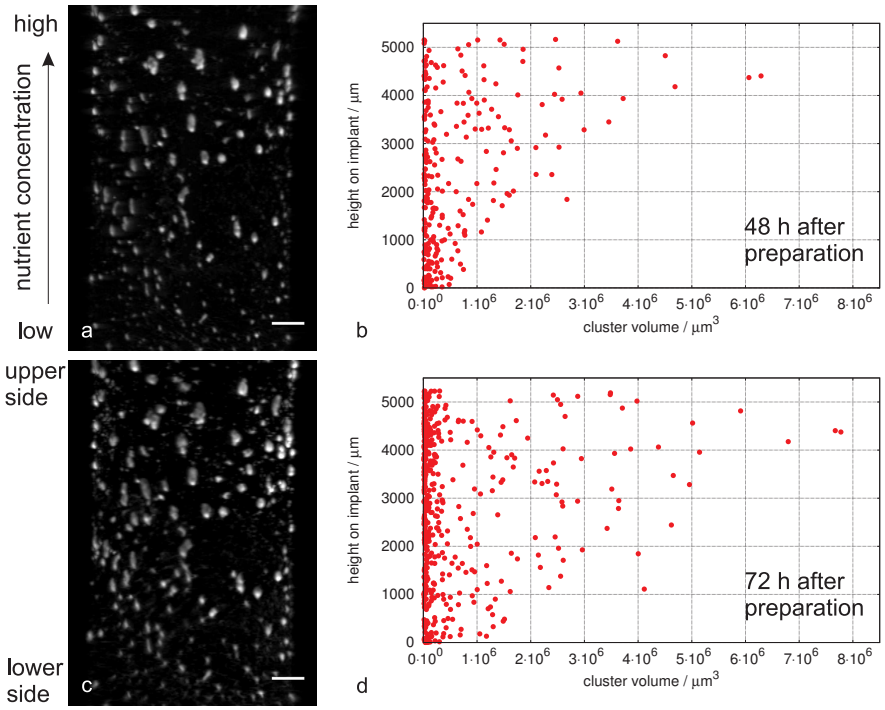


Figure 7. Analysis of biofilm clusters on a titanium cylinder at two points in time: Maximum intensity projection (left) and cluster volume as a function of height position on the implant surface (right) of reconstructed biofilm two days after preparation (a,b) and 24 h later (c,d). In accordance with the nutrient concentration gradient in the agarose gel, the cluster volume in the upper region is larger than in the lower region of the sample. The cluster number increases from 246 to 467 within 24 h. Biofilm: Extraction of patient's dental plaque. Scale bars represent 500 µm.

## 4. Discussion

SLOT is capable of visualizing the three dimensional biofilm structure *in vitro* on curved and non-transparent surfaces like dental implants by detecting scattered laser light only. While SLOT is originally a highly efficient fluorescence microscopy technique [19], it also succeeds when using absorption and scattering. These intrinsic contrast mechanisms allow the investigation of native specimen *in vitro* without the need for extensive vital staining with fluorescent markers. The SLOT setup presented here simultaneously detects transmitted and scattered light at a specific illumination laser wavelength. While the transmission channel likewise contains information about the absorption and scattering within the specimen, solely scattered light is detected by the PMT. However, in the case of non-transparent objects like implants the transmission channel may be corrupted due to shadowing effects caused by cavities on the surface: An incident beam carrying the information of structures within a cavity does not reach the PD causing the illusion of a plain surface instead of displaying the actual shape [26]. Scattered light on the contrary is guided along the water-filled cuvette towards the bottom and reaches the active area of the PMT positioned below the specimen. This is true for every position on

#152496 - $15.00 USD Received 8 Aug 2011; revised 2 Sep 2011; accepted 2 Sep 2011; published 3 Oct 2011

the non-transparent object independent of its surface characteristics. The position of the PMT below the sample is crucial since direct reflections of the illumination beam at the test tube onto the active area have to be avoided. These reflections would generate static stripes in the projection images causing severe reconstruction artifacts [27].

Beside the main advantages of SLOT compared to OPT namely homogeneous illumination, prevention of ring artifacts and a high collection efficiency [19] the SLOT setup additionally allows the image formation by detection of scattered laser light. In standard OPT the acquired projection images would be degenerated by speckle noise [28] due to the coherence length of the laser light being larger than the sample size. SLOT suppresses speckles because of the one dimensional detection with a high numerical aperture which corresponds to an integration of the scattered laser light intensity over a large solid angle. Out of this reason SLOT can acquire scattered light projection images at a specific wavelength by simply using a laser which is more efficient than applying a narrow band pass filter in combination with a light emitting diode (LED) in OPT. The above comparison of SLOT with OPT is also valid for simple white-light microscopy. A reflected-light microscope could be applied with a low NA in the detection path and extended by a rotation stage to acquire projection images of scattered light as presented in the results section. However, such a setup would be comparable to a OPT setup with the above discussed disadvantages compared to SLOT.

The application of the redox indicator TTC commonly used as a non-fluorescent viability marker in biochemical experiments [21, 23, 22] allows SLOT to easily differ between implant surface and biofilm. The latter consists of living bacterial cells that reduce the surrounding TTC during respiration and give the biofilm a visible red color. While the absorbance of the implant surface is nearly independent of the used wavelengths, the TPF produces a difference signal that permits the isolation of the biofilm for the subsequent reconstruction. On the other hand, light passing through the agarose undergo Rayleigh scattering with typical $\lambda^{-4}$ behavior resulting in a signal twice as high in the green channel (532 nm) compared to the red channel (633 nm). The difference signal data sets are equivalent to fluorescence projection data sets but do, however, not allow the differentiation between living bacteria species within the biofilm. TPF accumulates within every living cell in the prepared agarose while a specific biofilm constituent has to be fluorescently labeled for the detection with SLOT.

When using scattered light the SLOT setup has the same isotropic optical resolution of equivalent OPT setups. In the case of fluorescence detection the resolution is slightly higher in SLOT than in eOPT because in SLOT the optical resolution is determined by the excitation wavelength while in eOPT it is dependent of the emission wavelength [29, 19, 30]. For the imaging of a non-transparent cylinder the NA of the illumination beam is adjusted until the visible half of the implant is covered by the DOF. The required NA of 0.027 theoretically corresponds to an isotropic resolution of about 12 µm (at 633 nm) while covering a volume of 110 $mm^3$ compared to OCT systems with 25.6 $mm^3$ at < 20 µm [17] and about 8 $mm^3$ at 15 µm [15]. Concerning this theoretical comparison between OCT and SLOT it is important to mention their different relationships of measured volume and resolution. In OCT as in SLOT the measured volume depends on the size of the chosen scan area and the penetration depth at the used illumination wavelength. While OCT provides 3D data of a basically cuboid-shaped volume, SLOT measures a volume with cylindrical shape because of the rotation of the specimen. Thereby, the NA in the illumination path determines the lateral resolution in OCT and the isotropic optical resolution in SLOT, respectively. Due to the fact that in SLOT the NA has to be adjusted to yield a DOF spanning the specimen, the resolution is limited by the size of the measured volume. The axial resolution in OCT can be significantly higher than the lateral resolution, since it only depends on the wavelength and bandwidth of the used light source [31].

Low coherence interferometric techniques like OCT and LCI easily enable *in vivo* appli-

#152496 - $15.00 USD Received 8 Aug 2011; revised 2 Sep 2011; accepted 2 Sep 2011; published 3 Oct 2011

cations due to their ability to acquire tomographic data from backscattered light by using only one viewing direction [31, 18]. SLOT and OPT, on the other hand, require a set of projection images from 360 degrees to reconstruct volumetric data stacks and provide sectional views. Therefore, up to now only small specimens like the biological model organisms *D. melanogaster, C. elegans, P. hawaiensis* and zebrafish were investigated in *in vivo* OPT applications [32, 33, 34, 35, 36]. Since OPT and SLOT have similar specimen requirements, the application of SLOT for *in vivo* studies is limited in the same way as OPT.

The introduced sample preparation represents a test system that permits the *in vitro* evaluation of biofilm formation on dental implants. The sample mainly consists of a glass test tube containing a plastic tube with bacteria re-suspended in PBS, a Titanium metal cylinder or a dental implant respectively and the prepared agarose.

Enclosing and mounting the specimen within the glass tube avoids contamination and satisfies the requirements of the SLOT setup for mechanical stability and optical transparency. The glass tube may also be placed within an incubation chamber between measurements for long term observations. The plastic tube filled with PBS assures that the containing bacteria are placed at one end of the implant and can migrate along the surface through the gap between implant and surrounding agarose. The bacteria applied here had the purpose of demonstrating the capabilities of the system as test specimen and can be replaced by a specific dental biofilm in further studies.

The different used metal surfaces show that implants of various shape, material and roughness may be investigated. This is of high importance because it allows studies on variable implant properties influencing the biofilm formation like surface roughness, surface energy and material, chemical characteristics and special design features of implant-abutment configuration [37].

The agarose surrounding the implant meets multiple requirements: It holds the implant at a fixed position with the test tube and suppresses movement of the sample. Furthermore it is optically transparent in the investigated spectral range, has a low scattering coefficient and offers the refractive index of water. The latter is crucial to reduce mismatch artifacts due to reflection and distortion at the optical interfaces. Also, the agarose gel consists mostly of water providing an aqueous environment that keeps the biofilm in a hydrated state. This is of course essential for *in vitro* investigations just as well as the supply with nutrients: The described concentration gradient of TSB offers increasing developmental conditions which make sure that the biofilm grows and migrates along the implant. This is, however, a nonrealistic assumption related to the *in vivo* situation.

The use of tetrazolium salts like TTC for the staining of dehydrogenase activities is known since the 1940s [23, 22]. Beside other forms like INT, XTT and MTT, TTC is a standard indicator in biofilm growth experiments [38, 21, 39] measuring the optical absorbance. TTC is water soluble and colorless in its native form but forms red colored, water insoluble formazan if reduced. Due to the fact that only living cells are stained, TTC is used in various cell proliferation and toxicity assays and is therefore ideally suited for the *in vitro* investigation of biofilm growth without fluorescent markers.

The processed volumetric data stacks are useful for the objective evaluation of bacterial growth and supply raw material for quantitative parameter studies. 3D image analysis is essential for the quantitative and objective evaluation of volumetric biofilm data [40]. Recent works describe analysis software for the investigation of biofilm images obtained with confocal laser scanning microscopy (CLSM) [41, 42, 43]. Parameters used for the description of biofilm morphology in three dimensions are biovolume, volume to surface ratio, average biofilm thickness and distribution, volumes of micro-colonies at the substratum and their fractal dimension, distributions of diffusion distance, roughness coefficient and even more. Since large scale volu-

#152496 - $15.00 USD Received 8 Aug 2011; revised 2 Sep 2011; accepted 2 Sep 2011; published 3 Oct 2011

metric data stacks largely differ from data obtained with CLSM [17] 3D *in vitro* data of biofilm on implant surfaces acquired with SLOT may be investigated in terms of migration velocity, surface coverage ratios, biofilm mass distribution, detachment, porosity and density in future works.

## 5. Conclusion

Scanning laser optical tomography (SLOT) - originally a highly efficient 3D fluorescence microscopy technique - also succeeds when using absorption and scattering as contrast mechanism. It enables 3D imaging of specimen covering non-transparent and curved surfaces. Thus, the presented system, consisting of a SLOT setup and a biofilm test model as sample, is suitable for the large scale visualization of *in vitro* biofilm formation on dental implants. SLOT is capable of generating volumetric data stacks of biofilm by detecting wavelength-dependent scattered light. We suggest SLOT to be a valuable tool elaborating future studies on the structural and volumetric investigation of biofilm formation on implants at larger scales.

## Acknowledgments

This work has been supported by the excellence cluster Rebirth (From **Re**generative **Bi**ology to **R**econstructive **Th**erapy) and the Transregio 37 initiative, funded by the German Research Foundation (DFG). We would like to thank the program developers of the open source software ImageJ (rsbweb.nih.gov/ij/) and Voreen (www.voreen.org).

#152496 - $15.00 USD Received 8 Aug 2011; revised 2 Sep 2011; accepted 2 Sep 2011; published 3 Oct 2011